JOURNAL OF GEOPHYSICAL RESEARCH, VOL. 100, NO. B4, PAGES 5991–6003, APRIL 10, 1995

Seismic anisotropy of shales

Joel E. Johnston and Nikolas I. Christensen

Department of Earth and Atmospheric Sciences, Purdue University, West Lafayette, Indiana

Abstract. The seismic properties and preferred clay mineral orientation of a suite of shales are investigated using laboratory velocity measurements as a function of confining pressure, X ray diffraction techniques, and electron microprobe backscatter (BSE) imaging. The velocity measurements indicate that these shales are transversely isotropic with the main symmetry axis perpendicular to bedding. Anisotropy, at elevated pressures caused mainly by preferred orientation of clays (illite) parallel to bedding, ranges from 20% (V_p) and 19% (V_s) for a sample of New Albany Shale to 30% (V_p) and 35% (V_s) for a sample of Chattanooga Shale. The degree of clay mineral alignment in the shales is constrained by "orientation indices" produced using simple X ray diffraction techniques. A strong positive correlation is found between the degree of preferred orientation, as expressed in the orientation indices, and seismic anisotropy. BSE images of the shale fabrics confirm in a qualitative manner the results of the X ray study. To investigate wave propagation in the shales, elastic constants of each sample are calculated and used to produce phase and group (wave) velocity surfaces, which describe variation in velocity as a function of angle to the bedding normal. The calculated velocity surfaces, constrained by independent velocity measurements, display a lack of shear wave splitting at "near-normal incidence" in even the most anisotropic shales. For the highly anisotropic Chattanooga shales, group velocity surfaces differ significantly from corresponding phase velocity surfaces.

Introduction

Although shales comprise approximately 50% of the average sedimentary basin [*Boggs*, 1992] and are important hydrocarbon source rocks, relatively few studies have been undertaken dealing with their seismic properties. In addition to their abundance, shales often exhibit strong seismic anisotropy, a phenomenon that can have significant effects on seismic data [e.g., *Levin*, 1979; *White et al.*, 1983; *Banik*, 1984; *Winterstein*, 1986; *Brocher and Christensen*, 1990; *Lynn and Thomsen*, 1990; *Carrion et al.*, 1992]. Laboratory measurements of shale velocities and seismic anisotropy, important for the interpretation of field data, are relatively rare mainly due to the difficulty in working with samples that are often fissile and/or friable [e.g., *Jones and Wang*, 1981]. Investigations dealing with clay mineral alignment in shales, often cited as the underlying cause of their extreme anisotropy, are equally scarce.

For these reasons, we have undertaken a laboratory study of the seismic properties of shales using laboratory velocity measurements, X ray diffraction techniques, and electron microprobe imaging. Compressional and shear wave velocity measurements as a function of confining pressure indicate that these shales are transversely isotropic with the main symmetry axis perpendicular to bedding. Electron microprobe backscatter images and X ray diffraction methods have been used to quantify the degree of clay mineral alignment parallel to bedding in each sample, which in turn has been related to observed compressional and shear wave anisotropy. Elastic constants calculated for each of the samples have been used to produce velocity surfaces which describe variation in velocity as a function of angle to bedding normal. These surfaces, constrained by additional velocity measurements at a range of angles to bedding, indicate a lack of shear wave splitting or significant variation in compressional wave velocity for near-normal angles of incidence in even the most highly anisotropic shales. The results of this study show that detailed laboratory velocity measurements, in combination with simple techniques to quantify clay mineral alignment, can provide important information regarding anisotropy and wave propagation in fine grained sedimentary rocks.

Paper number 95JB00031.
0148-0227/95/95JB-00031$05.00

Previous Studies

Few laboratory studies have dealt extensively with seismic velocities in shales. In a pioneering study, *Kaarsberg* [1959] used atmospheric pressure compressional wave velocity measurements and X ray diffraction techniques (described in greater detail below) to examine clay mineral alignment in claystones and shales as a function of density and burial depth. *Podio et al.* [1968] examined the effects of water saturation and confining pressure on the velocities and elastic constants of a Green River Shale. *Jones and Wang* [1981] measured the velocities of two Cretaceous shales from the Williston basin. They found these rocks to be transversely isotropic with the main symmetry axis perpendicular to bedding. The transverse isotropy was attributed to clay mineral alignment parallel to bedding. Recently, *Vernik and Nur* [1992] measured the velocities of a suite of kerogen rich shales from the Williston basin. They related the anisotropy of the shales to their kerogen content and maturation level. Elastic constants were calculated for the shales, as were phase velocity surfaces for one of the samples. *Johnston and Christensen* [1994] measured the velocities of two highly anisotropic Chattanooga shale samples. Elastic constants of the shales were calculated and used to produce phase and group velocity surfaces for each. In addition to these studies, a number of papers have reported shale velocity-pressure data [e.g.,

Castagna et al., 1985; *Thomsen*, 1986; *Lo et al.*, 1986; *Rai and Hanson*, 1988; *Christensen and Szymanski*, 1991; *Freund*, 1992; *Johnston and Christensen*, 1992].

Sample Collection and Petrographic Descriptions

Samples for the present study were collected from three Devonian-Mississippian black shale formations. Two samples (TH-26 and TH-51) were obtained from the Chattanooga Shale (Millboro member) of eastern Tennessee, exposed in the Thorn Hill sedimentary section [*Walker*, 1985]. Four shales were collected from the New Albany Shale of the Illinois Basin, exposed in a southern Indiana quarry [*Lineback*, 1970; *Hasenmueller and Basset*, 1981]. Two samples (NEW2 and NEW3) were taken from the lowermost Blocher member of the New Albany, while the remainder (NEW5 and NEW7) were collected from the Morgan Trail member [*Lineback*, 1970]. Last, one sample of the lower Antrim Shale [*Matthews*, 1993] of the Michigan Basin was obtained from a quarry exposure in northern Michigan. All of the shales collected are extremely well indurated and thus ideally suited for laboratory study.

The mineralogy of each shale was examined using standard petrographic techniques, supplemented by X ray diffraction methods (described in greater detail below) and whole rock geochemical analyses. Brief petrographic descriptions and geochemical data for the shale suite are listed in Table 1. The dominant clay mineral in these shales is illite, with subordinate chlorite. Nonclay constituents include quartz, pyrite, dolomite, and minor calcite. Organic matter, seen as amorphous reddish brown material intermixed with the clay minerals, is common in all of the shales. The Chattanooga shales are distinguished from the rest of the samples in having greater amounts of chlorite, and in being especially rich in clays and organic matter with very fine grained quartz and pyrite as the only nonclay constituents. This is reflected in relatively high percentages of Al_2O_3 and K_2O (indicative of clays) and low percentages of SiO_2 (indicative of all silicate minerals, but very sensitive to quartz) for these samples [*Boggs*, 1992]. Occasional thin laminae of carbonate minerals (mainly dolomite) identified by petrographic means in NEW5 and NEW7 are expressed geochemically by relatively large percentages of CaO for these samples (Table 1). When viewed in polarized light in the petrographic microscope, the phenomenon of "mass extinction" [*Folk*, 1962; *Boggs*, 1992] is observed to some degree in all specimens, but is especially prominent in the Chattanooga shales, indicating very strong preferred orientation of clays parallel to bedding.

Experimental Techniques and Velocity Measurements

From each shale sample, multiple 2.54-cm-diameter cores were taken parallel, perpendicular, and at 45° to bedding. Cores were also taken at a range of other angles to bedding, usually in 10°-15° increments, depending upon the size of the sample. All cores were oriented very carefully with respect to the bedding plane (±0.5° for the 45° cores, ±1° for the remainder) to ensure that angles were "true" and accurate elastic constants would be obtained. The cores were then polished into right circular cylinders, with ends flat and parallel to within ±0.05 mm. A few cores fractured during preparation, and thus were discarded, but not enough to bias our analysis of a given shale sample. The lengths, diameters, and weights of the cores were measured to determine sample density. The velocity of

Table 1. Mineralogies and Whole Rock Major Element Analyses of Shale Samples

Sample	Mineralogy	Chemical Composition									Loss on Ignition	Total
		SiO_2	Al_2O_3	Fe_2O_3*	MgO	CaO	Na_2O	K_2O	TiO_2	P_2O_5	MnO	Cr_2O_3		
TH-26	illite,chlorite,quartz, pyrite	48.80	18.60	7.01	1.72	0.10	0.34	4.25	0.81	0.10	0.03	0.00	17.5	99.26
TH-51	illite,chlorite, quartz, pyrite	51.58	18.46	7.01	1.67	0.05	0.29	4.42	0.78	0.10	0.03	0.02	15.9	100.31
NEW2	illite,chlorite,quartz, pyrite, dolomite, calcite	65.59	12.07	4.27	1.04	0.06	0.30	3.47	0.59	0.04	0.01	0.02	12.8	100.26
NEW3	illite,chlorite,quartz, pyrite, dolomite	63.03	12.63	4.22	1.25	1.16	0.31	3.71	0.59	0.04	0.04	0.01	13.2	100.19
NEW5	illite,chlorite,quartz, dolomite,pyrite	62.15	10.79	4.31	1.96	2.97	0.29	3.06	0.49	0.05	0.06	0.01	13.6	99.74
NEW7	illite,chlorite,quartz, pyrite,dolomite, calcite	60.55	10.50	4.51	2.57	3.92	0.29	3.25	0.47	0.08	0.08	0.01	13.4	99.63
ANT1	illite,chlorite,quartz, pyrite	58.25	11.88	4.97	1.19	0.37	0.64	3.84	0.64	0.05	0.02	0.02	18.4	100.27

* Total Fe as Fe_2O_3.

Table 2. Physical Property Data for Shale Suite Including Densities (and Standard Deviations), Velocities for Select Propagation Directions, Anisotropies, X Ray Orientation Indices, Elastic Constants, and Anisotropy Parameters [*Thomsen*, 1986]

				Velocities, km/s								Anisotropy, %		Orientation	Elastic Constants (GPa)						Anisotropy Parameters	
				Perpendicular to Bedding		45° to Bedding			Parallel to Bedding													
Sample	Cores	Density g/cm³	Pressure MPa	V_p	V_s	V_p	V_{sh}	V_{sv}	V_p	V_{sh}	V_{sv}	V_p	V_s	Index	C_{11}	C_{12}	C_{33}	C_{44}	C_{13}	C_{13}(I)*	ε	δ
TH-26	13	2.341±0.030	10	2.850	1.710	3.560	2.302	1.990	4.404	2.744	1.707	35	38	161	45.40	10.15	19.02	6.83	8.60	8.76	0.69	0.20
			50	3.134	1.832	3.790	2.356	2.132	4.549	2.816	1.795	31	36		48.44	11.32	22.98	7.64	12.58	10.94	0.55	0.16
			100	3.286	1.886	3.912	2.397	2.189	4.666	2.864	1.844	30	35		50.96	12.55	25.28	8.08	13.90	12.40	0.51	0.14
TH-51	13	2.398±0.044	10	3.141	1.928	3.859	2.461	2.197	4.758	2.887	1.803	34	35	167	54.29	14.31	23.66	8.35	10.26	10.36	0.65	0.16
			50	3.299	1.980	3.973	2.553	2.310	4.891	2.968	1.857	33	35		57.37	15.12	26.10	8.82	10.88	10.88	0.60	0.10
			100	3.431	2.020	4.056	2.594	2.363	4.965	3.004	1.891	31	35		59.11	15.83	28.23	9.17	11.83	11.83	0.55	0.07
NEW2	13	2.268±0.011	10	2.978	1.907	3.388	2.214	2.063	3.975	2.501	1.968	25	23	22	35.84	7.46	20.11	8.46	5.06	6.27	0.39	0.17
			50	3.211	1.994	3.592	2.303	2.153	4.097	2.547	2.023	22	21		38.07	8.64	23.38	9.13	8.04	7.83	0.31	0.13
			100	3.369	2.071	3.737	2.374	2.225	4.215	2.595	2.085	20	20		40.29	9.75	25.74	9.78	9.43	8.68	0.28	0.10
NEW3	18	2.356±0.010	10	2.961	2.002	3.463	2.325	2.154	4.060	2.604	2.022	27	23	43	38.84	6.88	20.66	9.52	5.14	5.60	0.44	0.23
			50	3.213	2.079	3.662	2.401	2.246	4.209	2.672	2.094	24	22		41.74	8.10	24.32	10.24	7.67	7.53	0.36	0.17
			100	3.394	2.149	3.811	2.459	2.314	4.343	2.723	2.154	22	21		44.44	9.50	27.14	10.90	9.05	8.93	0.32	0.15
NEW5	20	2.370±0.008	10	3.061	2.095	3.592	2.381	2.210	4.135	2.615	2.091	26	20	21	40.52	8.11	22.21	10.38	6.73	6.08	0.41	0.25
			50	3.331	2.180	3.783	2.447	2.314	4.301	2.699	2.169	23	19		43.84	9.31	26.30	11.21	8.48	7.88	0.33	0.17
			100	3.507	2.250	3.935	2.505	2.382	4.424	2.754	2.239	21	19		46.39	10.44	29.15	11.95	10.12	9.18	0.30	0.15
NEW7	25	2.386±0.006	10	3.173	2.100	3.661	2.393	2.242	4.184	2.638	2.113	24	20	25	41.75	8.56	24.01	10.58	7.87	6.65	0.37	0.18
			50	3.433	2.188	3.842	2.463	2.340	4.361	2.712	2.195	21	19		45.36	10.28	28.11	11.45	9.04	8.75	0.31	0.14
			100	3.598	2.257	3.982	2.527	2.409	4.489	2.774	2.268	20	18		48.06	11.36	30.88	12.20	10.17	10.06	0.28	0.13
ANT1	21	2.212±0.006	10	2.747	1.751	3.223	2.038	1.900	3.744	2.344	1.742	27	25	59	31.01	6.70	16.69	6.75	6.83	6.05	0.43	0.20
			50	2.973	1.823	3.378	2.096	1.977	3.888	2.402	1.808	24	24		33.44	7.91	19.55	7.30	7.89	7.41	0.36	0.14
			100	3.142	1.871	3.505	2.152	2.042	4.019	2.454	1.863	22	24		35.73	9.09	21.84	7.71	8.74	8.66	0.32	0.11

*C_{13}(I) stands for "best fit" C_{13} (see text).

each core was then measured to confining pressures of 100 MPa using the pulse transmission technique and a mercury delay line [*Christensen*, 1985]. In general, three velocities were measured per core: the compressional wave velocity (V_p), the velocity of the shear wave vibrating parallel to bedding (V_{sh}), and the velocity of the shear wave vibrating in a plane perpendicular to bedding (V_{sv}). For cores taken perpendicular to bedding, the V_{sh}-V_{sv} distinction is obviously not used. Velocities were measured under unsaturated conditions, since all of the samples have porosities much less than 1%.

Velocities for selected propagation directions, anisotropies, densities, standard deviation of densities, and number of cores taken per shale are listed in Table 2. Note that the densities given are averages of all the core densities for that sample, and that the velocities listed are generally averages of several measurements. Compositional homogeneity in the samples is demonstrated by low standard deviations of mean density for each shale. The velocity data indicate that these shales are transversely isotropic with the main symmetry axis perpendicular to bedding (Figure 1). Some characteristics of a transversely isotropic solid include (1) compressional and shear wave velocities independent of propagation direction in the bedding plane and, (2) velocities of shear waves propagating perpendicular to bedding equal to the velocities of the shear waves propagating in the bedding plane, vibrating in a plane perpendicular to bedding [*Hearmon*, 1961; *Christensen*, 1966; *Musgrave*, 1970].

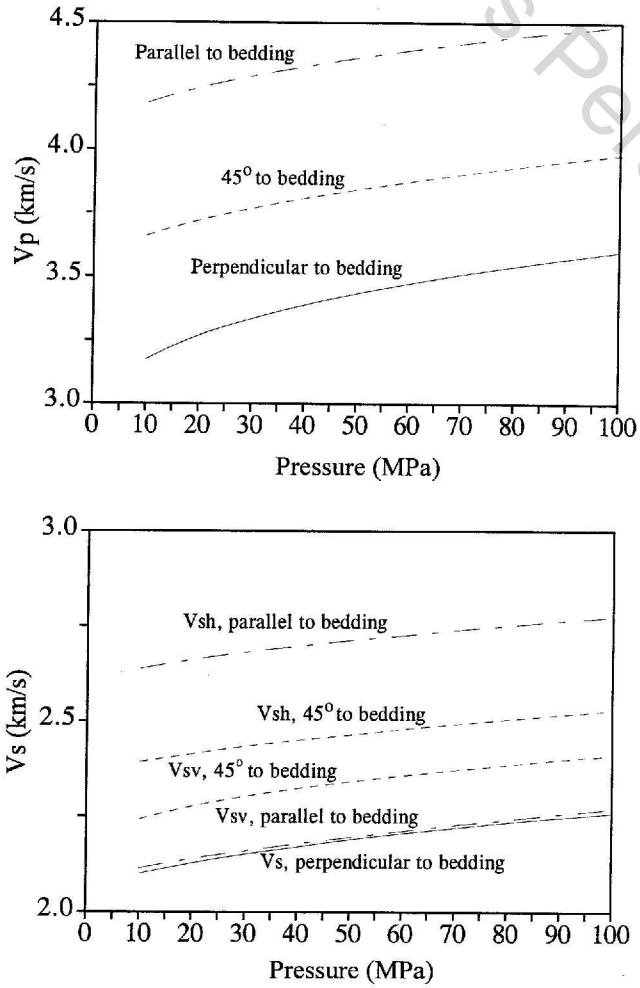

Figure 1. Compressional and shear wave velocities for select propagation directions as a function of confining pressure for NEW7. Each curve is an average of multiple measurements.

Anisotropy and Clay Fabric of Shales

In the present study, seismic anisotropy is defined in terms of symmetry direction velocity measurements as $(V_{max}-V_{min})/V_{max}$, expressed as a percent. The data given in Table 2 indicate that all of the shales examined are highly anisotropic. The Chattanooga shales, TH-26 and TH-51, exhibit extreme anisotropy, approximately 30% for V_p and 35% for V_s at 100 MPa. The remainder of the shales from the New Albany and Antrim formations all possess approximately 20% V_p and V_s anisotropy, although ANT1 and NEW3 are slightly more anisotropic than NEW2, NEW5, and NEW7. Anisotropy is observed to decrease slightly with increasing confining pressure for each sample. At low confining pressures (~10 MPa), aligned microcracks and preferred orientation of clay minerals contribute to the observed anisotropy. As confining pressure is increased, anisotropy decreases due to closure of microcracks. At 100 MPa, observed anisotropy can mainly be attributed to clay mineral alignment parallel to bedding, although there could probably still be a small contribution due to the few microcracks which remain open.

Although preferred orientation of clay minerals has often been cited as the dominant cause of seismic anisotropy in shales [e.g., *Jones and Wang*, 1981; *Vernik and Nur*, 1992; *Johnston and Christensen*, 1994], no direct investigation of this relationship has been attempted. In the present study, two complementary techniques, X ray diffraction and electron microprobe imaging, have been used to examine clay fabric in these Devonian-Mississippian shales. X ray diffraction has been used to provide a relative estimate of clay mineral alignment parallel to bedding which has then been confirmed using electron microprobe backscatter images.

X Ray Diffraction

Many studies have used X ray diffraction methods to investigate clay mineral alignment in clays and shales [e.g., *Kaarsberg*, 1959; *Silverman and Bates*, 1960; *Meade*, 1961; *O'Brien*, 1964; *Gipson*, 1966; *Odom*, 1967]. The only study to relate clay mineral alignment in shales, although indirectly, to laboratory velocity data was by *Kaarsberg* [1959]. Kaarsberg observed that sections taken parallel to bedding in shales produce prominent illite basal plane 002 diffraction peaks when X rayed, and from this observation formulated the idea of using X ray diffraction to study clay mineral alignment in clays and shales as a function of density and depth of burial. Kaarsberg found that studying illite alignment was ideal, since the 002 and 110 planes of this mineral are nearly at right angles to each other. Thus the greater the illite 002 planes are aligned parallel to bedding in a sample, the greater the 110 planes will be aligned perpendicular to bedding [*Kaarsberg*, 1959]. Kaarsberg's work provided the inspiration for using X ray diffraction techniques to investigate clay mineral alignment in the present study.

For each of the seven shales, 2.54-cm-diameter disks were cut from the ends of the cores taken parallel and perpendicular to bedding. These disks were then repolished until both sides of each disk had a mirrorlike finish. Polishing was done carefully to ensure that the surfaces of the disks retained their original orientation either parallel or perpendicular to bedding. The disks were then irradiated using a Phillips-Norelco X ray dif-

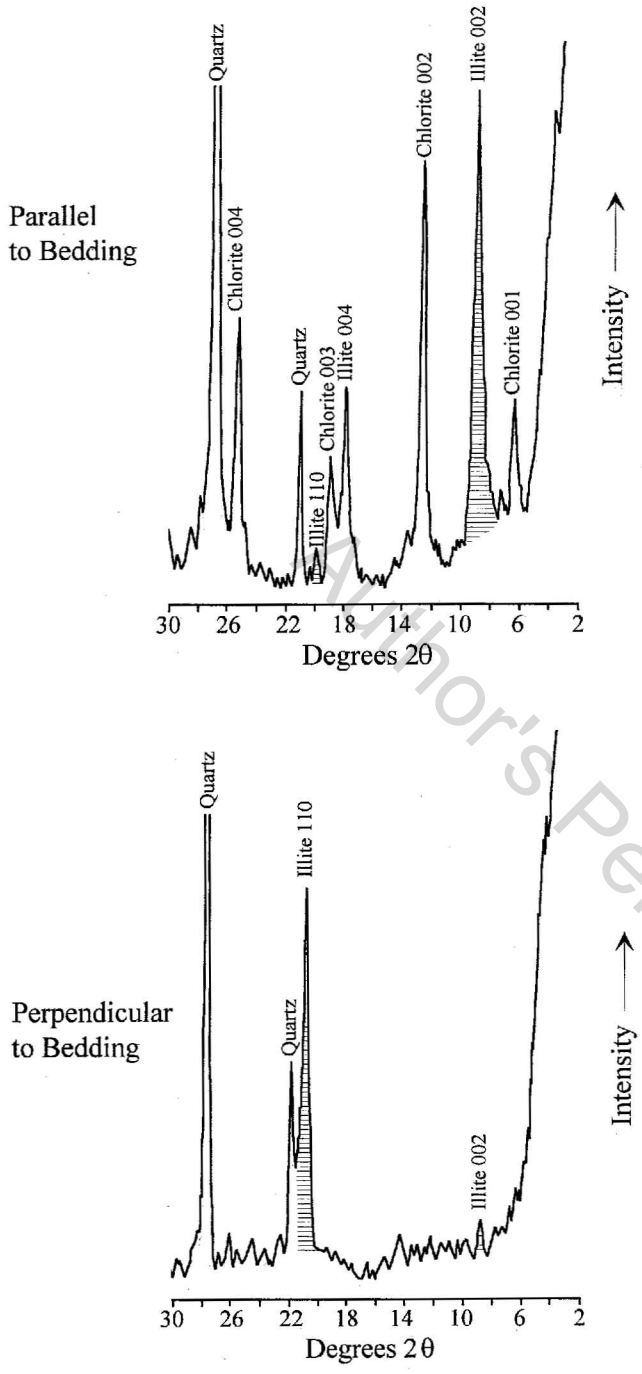

Figure 2. X ray diffraction traces (sections parallel and perpendicular to bedding) for TH-51. Illite 002 and 110 peaks are shaded.

fractometer (CuKα radiation), taking care to ensure that irradiated surface area was kept constant from sample to sample. The various mineral types were identified using standard procedures [e.g., *Moore and Reynolds*, 1989], paying particular attention to the diffraction peaks for the illite 002 and 110 planes. Figures 2 and 3 show typical X ray diffraction patterns for shales NEW2 and TH-51. For TH-51 (Figure 2), the section taken parallel to bedding produces a very strong illite 002 diffraction peak and a very weak illite 110 peak. Conversely, the section perpendicular to bedding produces a very strong 110 peak and a very weak 002 peak. These observations indicate that illite 002 planes in sample TH-51 are strongly aligned parallel to the bedding plane. The same overall differences between 002 and 110 peak intensity, although more subdued, are observed in the parallel and perpendicular sections of NEW2 (Figure 3), indicating that the illite flakes in NEW2 are not as well aligned as those in TH-51.

To obtain a relative measure of clay mineral alignment parallel to bedding in these shales, the method proposed by *Meade* [1961] has been adopted, which is a variation of the technique used by *Kaarsberg* [1959]. For a given shale, the average ratio of the 002 to 110 diffraction peak heights was calculated for the sections oriented parallel to bedding. This number was then divided by the average ratio of the 002 to 110 peaks for the sections perpendicular to bedding, producing an orientation index as follows:

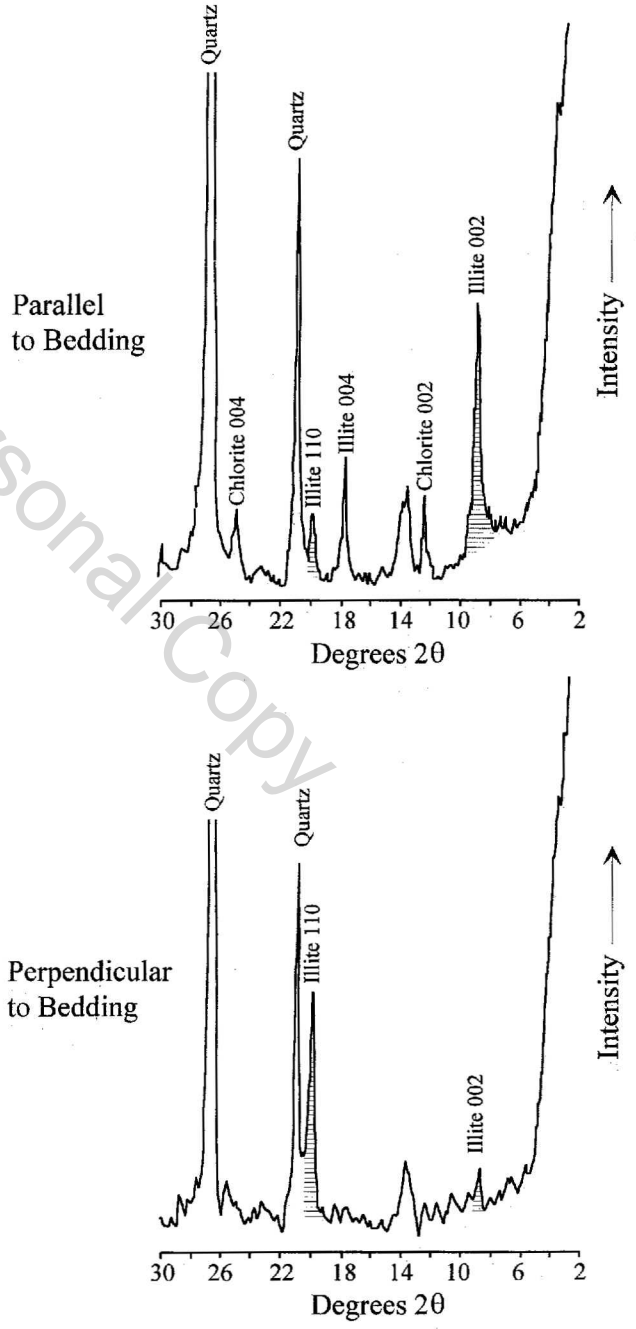

Figure 3. X ray diffraction traces for NEW2. Illite 002 and 110 peaks are shaded.

$$\text{Orientation Index} = \frac{(002/110)\text{ parallel to bedding}}{(002/110)\text{ perpendicular to bedding}}$$

The greater the degree of clay mineral alignment parallel to bedding in a sample, the greater the orientation index. A shale with randomly oriented clay particles would have an orientation index of approximately 1 [*Meade*, 1961]. The advantages of using this technique for investigating clay mineral alignment in shales include the fact that it is relatively simple, utilizes a maximum of information (sections both parallel and perpendicular to bedding are irradiated), and most important, other factors which affect peak intensity, including clay particle size, degree of crystallinity, sample thickness, etc., are canceled out [*Meade*, 1961; *Moore and Reynolds*, 1989].

Orientation indices for each of the shales, corrected for X ray noise, are listed in Table 2. The orientation indices indicate that all of the shales exhibit a high degree of illite alignment parallel to bedding. The Chattanooga shale samples, TH-26 and TH-51, exhibit the greatest degree of alignment, as indicated by very large orientation indices relative to the other shales. Samples NEW2, NEW5, and NEW7 have more random orientations of clay particles relative to the bedding plane, while NEW3 and ANT1 have clay alignments intermediate between these two extremes, as indicated by intermediate orientation indices.

In Figure 4, compressional and shear wave anisotropies of the shales at 100 MPa are plotted against respective orientation indices. A strong positive correlation is apparent, with the highly anisotropic Chattanooga shales having the largest orientation indices. NEW2, NEW5, and NEW7, the shales with the lowest anisotropy, form a cluster at the lower left corner of this plot, while NEW3 and ANT1 which have intermediate V_p and V_s anisotropies, and orientation indices, fill the gap between these two extremes.

Directly relating orientation indices to anisotropy as in Figure 4 ignores the fact that illite content varies from shale to shale. This could be a problem, since a very silty shale will exhibit low anisotropy even if all of its clay minerals are perfectly aligned. To account for variable clay content, the combined Al_2O_3 and K_2O contents (Table 1) of each shale, the oxides most

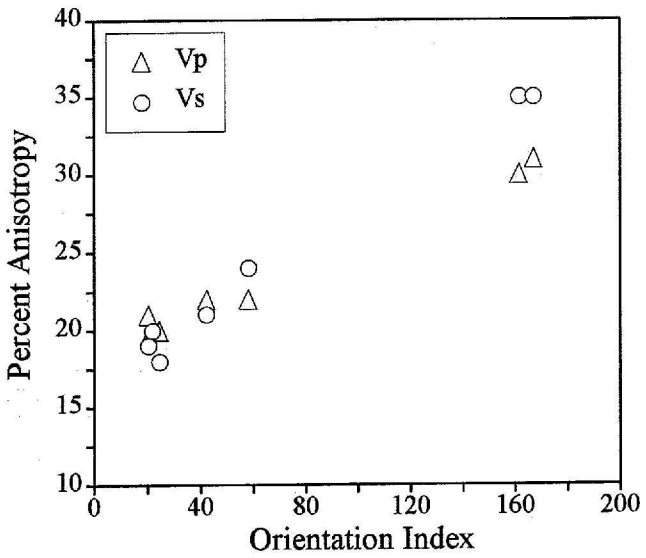

Figure 4. Percent compressional and shear wave anisotropy (100 MPa) of shales versus X ray orientation indices.

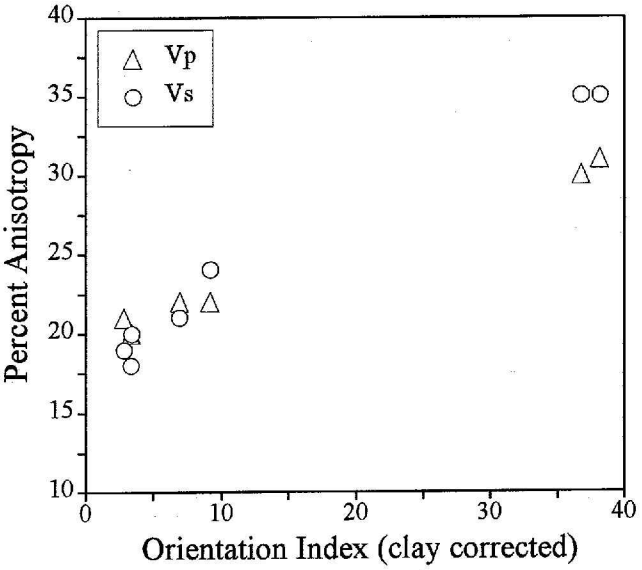

Figure 5. Percent compressional and shear wave anisotropy (100 MPa) of shales versus "clay content corrected" orientation indices.

indicative of clay minerals [*Boggs*, 1992], can be multiplied against the orientation indices. Thus shales with high clay contents will have relatively unchanged orientation indices while more quartz (or carbonate) rich samples will have reduced orientation indices. A plot of "clay corrected" orientation indices versus anisotropy is given in Figure 5. Very slight improvements to the overall linear trends of Figure 4 are apparent.

The correlation between orientation index and seismic anisotropy observed in Figures 4 and 5 is striking. Thus at elevated confining pressures, the observed anisotropy in these shales can be attributed dominantly to clay mineral alignment parallel to bedding, with greater degrees of alignment resulting in higher anisotropy. The degree of illite alignment is effectively characterized, in a relative sense, by the orientation index proposed by *Meade* [1961]. It should be pointed out that preferred orientation of nonclay minerals such as quartz cannot be ascertained by this method, but the effects of any such alignment on observed anisotropy are likely to be minimal relative to the clay contribution. In addition, chlorite is obviously a significant component of the Chattanooga shales (Figure 2). Since this clay does not have prominent nonbasal diffraction peaks [*Kaarsberg*, 1959], its alignment cannot be studied using either Kaarsberg's or Meade's techniques. It is probably safe to assume, however, that for a given sample, the chlorite is aligned parallel to bedding to the same degree as the surrounding illite.

Electron Microprobe Imaging

Scanning electron microscope (SEM) and electron microprobe investigations of shale fabric have primarily been confined to sedimentary petrology/petrography studies [e.g., *Gipson*, 1965; *O'Brien*, 1970; *White et al.*, 1984; *O'Brien*, 1986]. For example, *Gipson* [1965] used the SEM to study the sand, silt, and clay-sized particle orientation in shales. *White et al.* [1984] demonstrated the utility of the electron microprobe in backscatter mode for petrographic investigations of sandstones and shales. Recently, *O'Brien* [1986] used X-radiography and SEM images to examine bioturbation in shales. Limited use of electron microprobe and/or SEM images of shale fabric in relation

to seismic anisotropy has been undertaken in a few laboratory studies [*Jones and Wang*, 1981; *Vernik and Nur*, 1992].

To supplement the clay orientation information derived from X ray methods in the present study, a Cameca SX-50 electron microprobe operating in backscatter mode was used to collect digital images of the clay fabrics in each of the shales. Polished sections for the microprobe were made from disks cut from core ends. To obtain the best view of clay alignment, most of the sections were taken in a plane perpendicular to bedding. For comparison purposes, one polished section oriented parallel to bedding was prepared for sample TH-26. Several sites were examined in each polished section using the microprobe; at each site, digital images were collected at 100×, 200×, 500×, and 1000× magnification. The 500× and 1000× images were found to be most suitable in terms of resolution for examining clay mineral alignment. Only minor image processing was undertaken, primarily to increase tone contrasts between minerals. In a backscatter (BSE) image, the tone of a mineral is determined by its mean atomic number; the higher the mean atomic number, the brighter the mineral will appear. For example, pyrite, which has a mean atomic number (Z) of 20.65, appears white on BSE images, while quartz ($Z=10.80$), dolomite ($Z=10.87$), and illite ($Z=11.16$) are characterized by much darker tones [*White et al.*, 1984].

a).

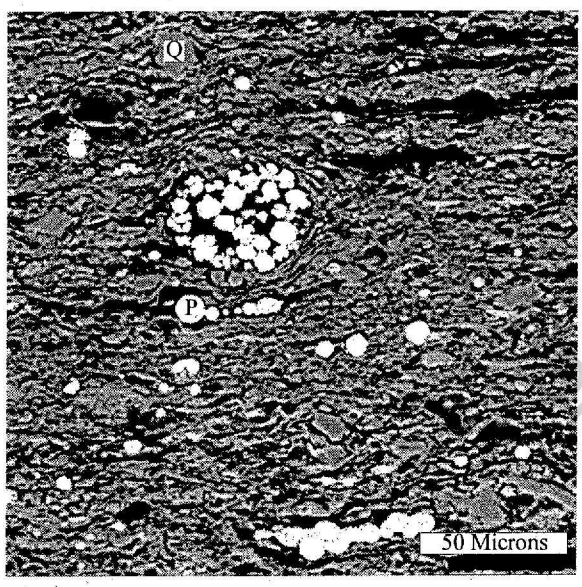

b).

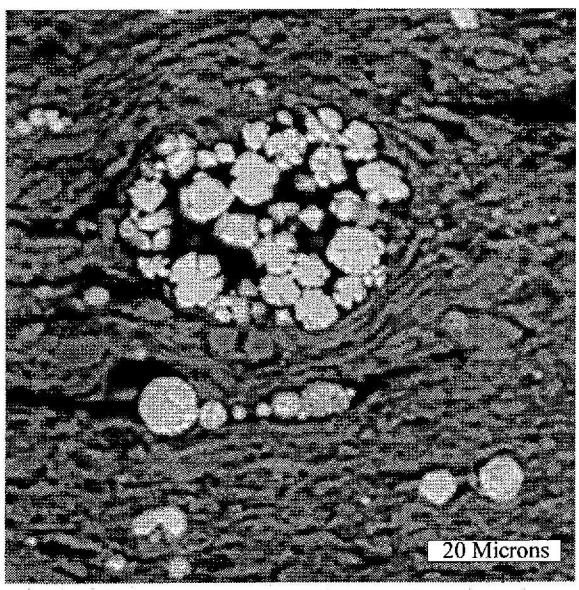

Figure 6. Electron microprobe backscatter (BSE) images of TH-26 taken in a plane perpendicular to bedding at (a) 500×, and (b) 1000×, magnification. In Figure 6a, select quartz (Q) and pyrite (P) grains are labeled.

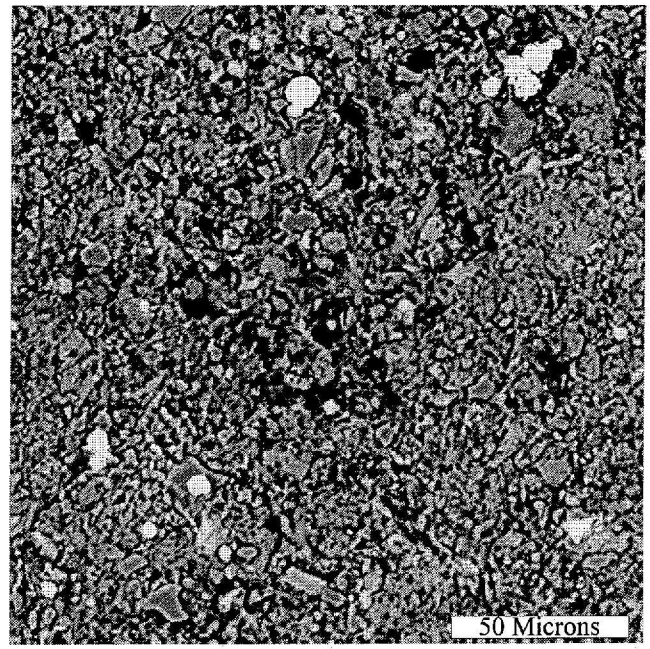

Figure 7. BSE image of TH-26 taken in a plane parallel to bedding at 500× magnification. Note lack of apparent preferred orientation of clay minerals.

A BSE image of Chattanooga shale TH-26, taken at 500× magnification in a plane perpendicular to bedding, is shown in Figure 6a. Pyrite grains are easily identified by their light tone and morphology. Quartz grains are identified by their darker tones, angular morphology, and the fact that softer clay minerals are often bent around them. Bright rims around the edges of quartz grains are distinctive of this mineral; even after careful polishing, the edges of hard minerals tend to stand higher than surrounding clay minerals and hence strongly reflect incident electrons [*White et al.*, 1984]. Though the borders of individual clay minerals are difficult to resolve, strong preferred orientation of clay minerals parallel to bedding is apparent. This alignment is emphasized by abundant lenses of organic matter oriented parallel to bedding, which appear black. An image of the same site at 1000× magnification (Figure 6b) emphasizes the preferred orientation and also shows compaction and bending of clay minerals around the harder pyrite grains. Equally strong clay mineral alignment parallel to bedding is apparent in BSE images of TH-51.

A BSE image of TH-26, taken at 500x magnification in a plane parallel to bedding (Figure 7) provides a strong contrast to Figure 6. Grains of bright pyrite and angular quartz are again visible. The majority of the image, however, is taken up by irregularly shaped clay minerals which display no apparent preferred orientation, as would be expected.

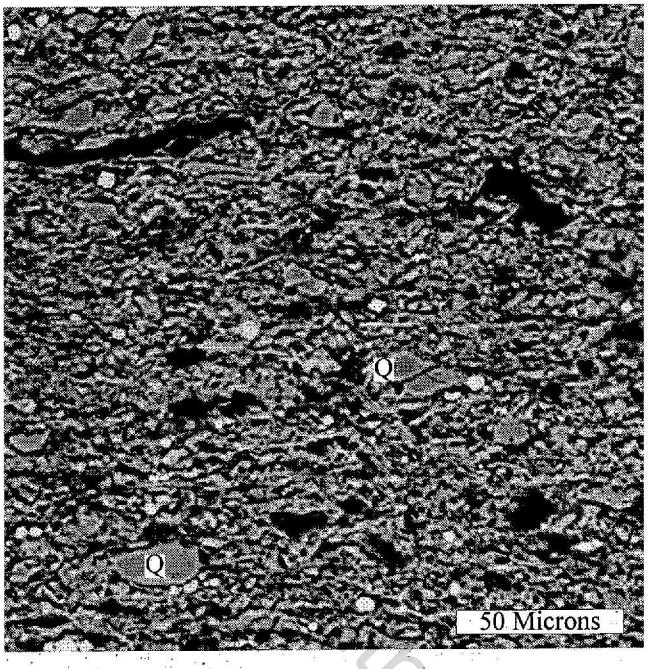

Figure 8. BSE image of NEW3 taken in a plane perpendicular to bedding at 500x magnification. Note abundant angular quartz grains.

The relatively poor alignment of clay minerals parallel to bedding in the New Albany and Antrim shale samples, as previously identified through the X ray measurements, is apparent on BSE images. A backscatter image of NEW3 (500×, section through bedding) is given in Figure 8. Note the significant number of angular quartz grains relative to the TH-26 images. Preferred orientation of clay minerals can be seen but is definitely not as prominent as in the Chattanooga shales. A similar degree of alignment can be seen in Figure 9, which displays images of NEW2 at 500× and 1000× magnification. As in Figure 8, a large number of nonclay minerals such as quartz and pyrite are visible which would partially account for the low anisotropy exhibited by these samples relative to the Chattanooga shales.

The BSE images presented above confirm in a qualitative manner the conclusions derived from X ray diffraction. All of the shales display prominent preferred orientation of clay minerals parallel to bedding, with very strong clay fabrics apparent in the Chattanooga Shale samples. The few microcracks observed in the BSE images were found to be aligned subparallel to bedding. Thus, at low confining pressures, the clay fabric and microcracks contribute to the observed transverse isotropy of the shales; at higher confining pressures (~100 MPa), where the majority of microcracks are closed, the effect of the preferred orientation of clays is dominant. It should be noted here that fine scale interlayering of dissimilar minerals (i.e., calcite and clay) has been identified as a source of seismic anisotropy (periodic thin layering anisotropy) in some deep-sea sediments by *Carlson et al.* [1984]; this phenomenon is believed to be insignificant in the present study.

The potential of BSE images and X ray diffraction for investigating preferred orientation of clays in relation to seismic anisotropy has been demonstrated in the first half of this paper. In the following sections, wave propagation in these shales will be examined through the calculation of elastic constants and velocity surfaces.

Elastic Constants

A transversely isotropic medium is described by five independent elastic constants [*Hearmon*, 1961]. Figure 10 shows schematically the key velocity measurements necessary for the calculation of the elastic constants in relation to the bedding plane of a shale. The actual velocity-elastic constant relationships [*Hearmon*, 1961; *Auld*, 1990] are as follows, where ρ is sample density:

$$C_{11} = \rho V_{p\,par}^2$$

$$C_{12} = C_{11} - 2\rho V_{sh}^2$$

$$C_{33} = \rho V_{p\,per}^2$$

$$C_{44} = \rho V_s^2$$

$$C_{13} = -C_{44} + [4\rho^2 V_{p\,45}^4 - 2\rho V_{p\,45}^2 (C_{11} + C_{33} + 2C_{44}) + (C_{11} + C_{44})(C_{33} + C_{44})]^{1/2}$$

a).

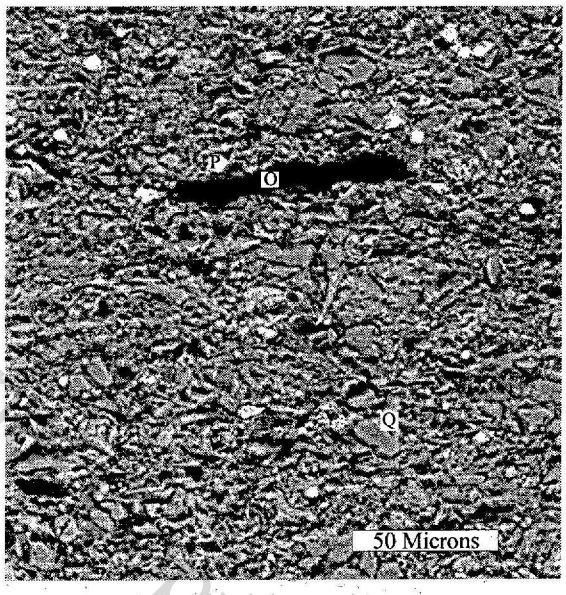

b).

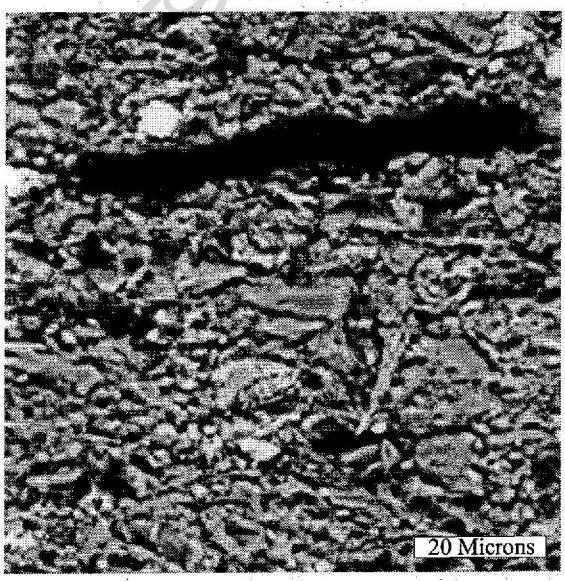

Figure 9. BSE images of NEW2 at (a) 500×, and (b) 1000×, magnification. Note pyrite (P), quartz (Q), and organic matter (O).

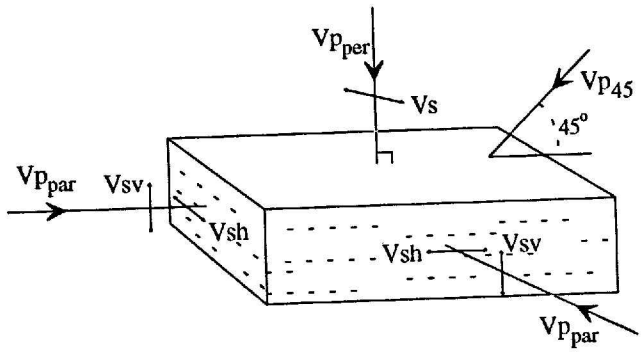

Figure 10. Schematic diagram of a shale sample relating critical velocity measurements to shale fabric. Note that for a transversely isotropic shale $V_s = V_{sv}$.

The calculations for the C_{11}, C_{12}, C_{33}, and C_{44} elastic constants are dependent on velocities measured along "symmetry" directions, either parallel or perpendicular to bedding. The relatively complex equation for the C_{13} constant is dependent upon measuring a compressional wave phase velocity (V_{p45}) in the cores taken at 45° to bedding. It has been demonstrated that standard laboratory velocity measurements on nonsymmetry direction cores record phase velocity [*Dellinger and Vernik*, 1994; *Johnston and Christensen*, 1994]. Phase velocity is defined as the speed with which seismic wave fronts travel in a direction parallel to the wave front normal [*Winterstein*, 1990]. Most laboratory velocity transducers can be considered planar sources and receivers [*Auld*, 1990]. Although the energy of the output transducer will tend to slip sideways as it travels down a nonsymmetry direction core, the dimensions of the core (2-4 cm long, 2.54-cm diameter) and transducers (2.54-cm diameter) are such that the flat portions of the output wave front will strike the receiving transducer (Figure 11). Thus, a phase velocity is measured, and calculation of C_{13} using the velocity-stiffness relation given above is justified. Elastic constants for the shale suite as a function of confining pressure are listed in Table 2.

Phase Velocity Surfaces

To describe three-dimensional wave propagation in these transversely isotropic shales, phase velocity surfaces were calculated using the Kelvin-Christoffel equations [e.g., *Auld*, 1990] and the elastic constants of each sample. These surfaces describe variation in phase velocity as a function of angle to bedding normal [*Winterstein*, 1990]. Three phase velocity surfaces are calculated: one for the quasi-compressional wave (V_p), one

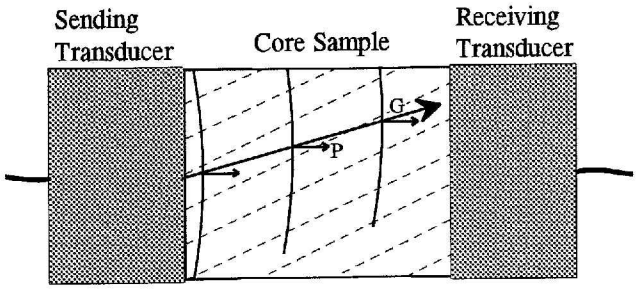

Figure 11. Schematic diagram of wave propagation in a nonsymmetry direction core where bedding is indicated by dashed lines. "P" indicates wavefront normal/phase velocity vector, "G" indicates related group velocity vector.

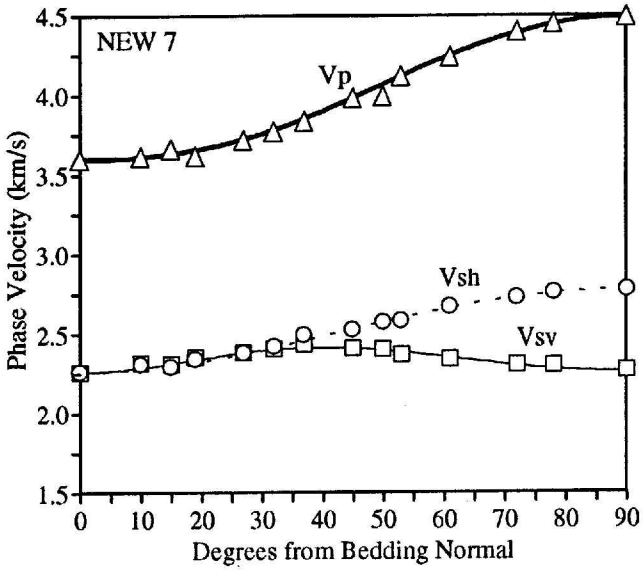

Figure 12. Phase velocity surfaces for NEW7. Measured velocities are shown as symbols, calculated velocities are shown as bold (V_p), thin (V_{sv}), and dashed (V_{sh}) lines. Note good agreement between calculated velocity surfaces and measured velocities.

for the shear wave vibrating parallel to bedding (V_{sh}), and one for the quasi-shear wave vibrating in a plane perpendicular to bedding (V_{sv}). Note that for propagation along symmetry axis directions (parallel or perpendicular to bedding), all wave modes are pure [*Auld*, 1990].

Phase velocity surfaces for samples NEW7, ANT1, and TH-26 at 100 MPa are shown in Figures 12-14. Measured velocities are shown as symbols and calculated velocities are shown as bold (V_p), thin (V_{sv}), and dashed (V_{sh}) lines. The calculated velocity surfaces, in conjunction with the measured velocities, display several interesting features concerning wave propagation in transversely isotropic rocks. For example, although each of the shales possesses strong shear wave anisotropy, there is no

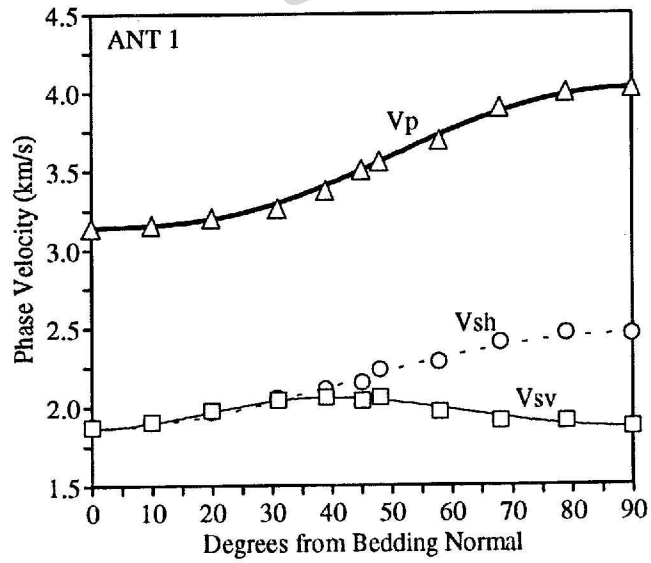

Figure 13. Phase velocity surfaces for ANT1. Note good agreement between calculated and observed velocities.

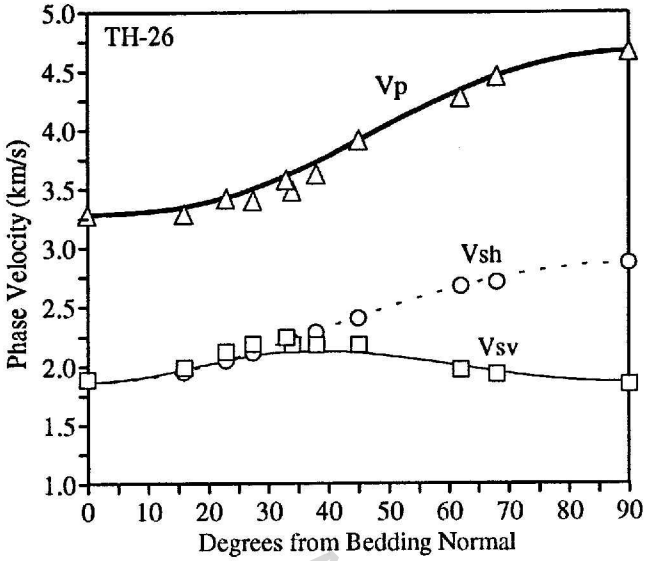

Figure 14. Phase velocity surfaces for TH-26. Note relatively poor agreement between calculated and observed V_p and V_{sv} phase velocities.

significant shear wave splitting for propagation directions 0-30° from the bedding normal. In this angular range, V_{sv} phase velocity is equal to if not slightly greater than V_{sh} phase velocity. Compressional wave phase velocity does not increase significantly until propagation directions greater than about 20° from bedding normal are reached. A dramatic peak in V_{sv} phase velocity, especially prominent for TH-26, is observed at approximately 40° from the bedding normal in each shale. Similar features are observed in the phase velocity surfaces for the other shales.

The independent nonsymmetry direction velocity measurements can be used to provide important checks on the validity of calculated velocity surfaces. Average differences between the independently measured phase velocities and corresponding calculated phase velocities for all samples are given in Table 3. For most of the shales the calculated and observed velocities agree very well, indicating that the calculated elastic constants are accurate and representative of the samples. However, systematic differences can be seen between the calculated and observed V_p and V_{sv} velocities for TH-26 (Figure 14), a sample for which only one 45° core was obtained. This observation can be explained as follows. The C_{11}, C_{12}, C_{33}, and C_{44} elastic constants of each shale are well constrained by multiple velocity measurements. More uncertainty is associated with the C_{13} constants because of the complex equation used in their calculation. If the 45° V_p phase velocity measurements are not representative of a given sample due to compositional heterogeneity or slight misorientations of the 45° cores, large errors can be propagated into C_{13} and the corresponding V_p and V_{sv} phase velocity surfaces. Fortunately, the overall accuracy of the C_{13} constants can be checked. Since only the V_p and V_{sv} phase velocity surfaces are dependent upon C_{13} [*Auld*, 1990], we can take advantage of the independent nonsymmetry direction velocity measurements by iteratively adjusting the C_{13} constant until a "best fit" is obtained between calculated and observed V_p and V_{sv} phase velocities. The iterative C_{13} constants are given in Table 2. With the exception of TH-26, the iterative C_{13} constants do not differ significantly from the directly measured constants, emphasizing the overall homogeneity of the samples and the accuracy of the critical 45° core velocity measurements.

Table 3. Average Differences (in km/s) Between Calculated Phase Velocities and Independent Nonsymmetry Direction Velocity Measurements

Sample	$\lvert V_{calc.}-V_{meas.}\rvert$, km/s		
	V_p	V_{sh}	V_{sv}
TH-26	0.064	0.015	0.065
TH-51	0.059	0.054	0.044
NEW2	0.016	0.024	0.017
NEW3	0.019	0.016	0.016
NEW5	0.023	0.014	0.037
NEW7	0.017	0.010	0.012
ANT1	0.018	0.018	0.013

Group Velocity Surfaces

Group (ray) velocity is defined as the speed with which a wave surface travels in a given direction radially outward from a point source in an anisotropic medium [*Winterstein*, 1990]. Group velocity (wave) surfaces for an anisotropic solid are derived mathematically from corresponding phase velocity surfaces by converting individual phase velocity vectors into their related group velocity vectors using the equations in *Hearmon* [1961] and *Musgrave* [1970]. In a graphical sense, group velocity surfaces are best visualized as being formed by constructive interference of plane waves emanating from a point source imbedded in an anisotropic solid [*Winterstein*, 1990]. Motivation for calculating group velocity surfaces is provided by the fact that in field studies, where point sources and receivers are used, group velocities are measured [e.g., *Thomsen*, 1986].

Group velocity surfaces for NEW7 and TH-26 are given in Figure 15. Previously calculated phase velocity surfaces are shown for reference. Note that along symmetry directions where wave modes are pure, group velocities are equivalent to phase velocities [*Winterstein*, 1990]. The group velocity surfaces of NEW7 and TH-26 display the same general features as the corresponding phase velocity surfaces in terms of shear wave splitting and variation of V_p at near-normal incidence. For sample NEW7 (Figure 15a), which possesses 20% V_p and 18% V_s anisotropy at 100 MPa, there is little difference between the group and phase velocity surfaces, especially for the V_{sv} wave mode. For highly anisotropic TH-26 (Figure 15b), however, group velocities are significantly less than phase velocities (at a given angle from bedding normal) for all three wave modes. Note the "cusp" present in the V_{sv} group surface, indicating that it may be possible to record multiple pulses of V_{sv} wave energy in properly designed field studies over highly anisotropic rocks.

In Figure 16, the group velocity surfaces of NEW7 and TH-26 are replotted to show the actual shape of the wave surfaces (in a plane perpendicular to bedding) which would radiate from a point source in each shale. The V_{sh} wave surfaces in transversely isotropic media are always ellipsoidal in shape [e.g., *Postma*, 1955; *Musgrave*, 1970]. The V_p wave surfaces of both shales superficially resemble ellipsoids, but are actually nonelliptical; this is especially true for highly anisotropic TH-26 (Figure 16b). The V_{sv} wave surfaces of Figure 16 are neither

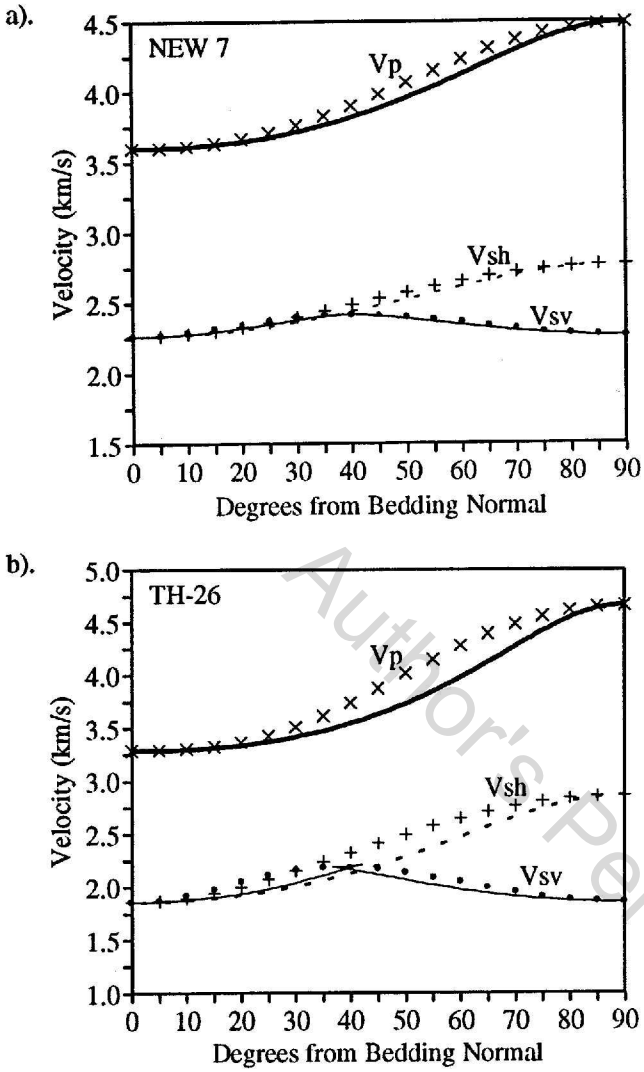

Figure 15. Group velocity surfaces (solid and dashed lines) for (a) NEW7 and (b) TH-26. Previously calculated phase velocity surfaces shown for reference as symbols in 5° increments.

elliptical nor circular, with shapes that defy simple geometric descriptions. However, for the V_{sv} wave mode, as well as the V_p and V_{sh} wave modes, the group velocity surfaces of Figure 16 describe a smooth, gradual increase in velocity at near-normal incidence.

Conclusions

In this study we have used a variety of complementary techniques to investigate the seismic properties of shales, including velocity measurements as a function of confining pressure, X ray diffraction, and electron microprobe imaging. The goals of this investigation have been twofold: to investigate the cause of seismic anisotropy in shales, and to describe wave propagation in these rocks.

We have demonstrated that simple X ray diffraction techniques, coupled with electron microprobe backscatter imaging, can effectively provide a relative measure of the degree of preferred orientation of clay minerals in shales. This preferred orientation can then be directly related to observed seismic anisotropy. Work done in this area, outside of *Kaarsberg's* [1959] study, has been relatively limited. Recently, *Sayers* [1994] has outlined a method for relating the clay particle orientation distribution function in shales to observed anisotropy. Additional studies expanding on the use of X ray and SEM techniques for examining the fabric of fine-grained sedimentary rocks are needed. However, it can be concluded from our study of shale fabric that preferred orientation of clay minerals is obviously a widespread and significant source of seismic anisotropy in sedimentary basins. Any interpretation of observed anisotropy (e.g., shear wave splitting) in sedimentary strata attributed solely to preferred crack orientation must be viewed with caution.

We have shown that careful laboratory velocity measurements on homogenous shale samples can be used to obtain very accurate elastic constants. Critical to this is the careful orientation of core samples with respect to the bedding plane and ve-

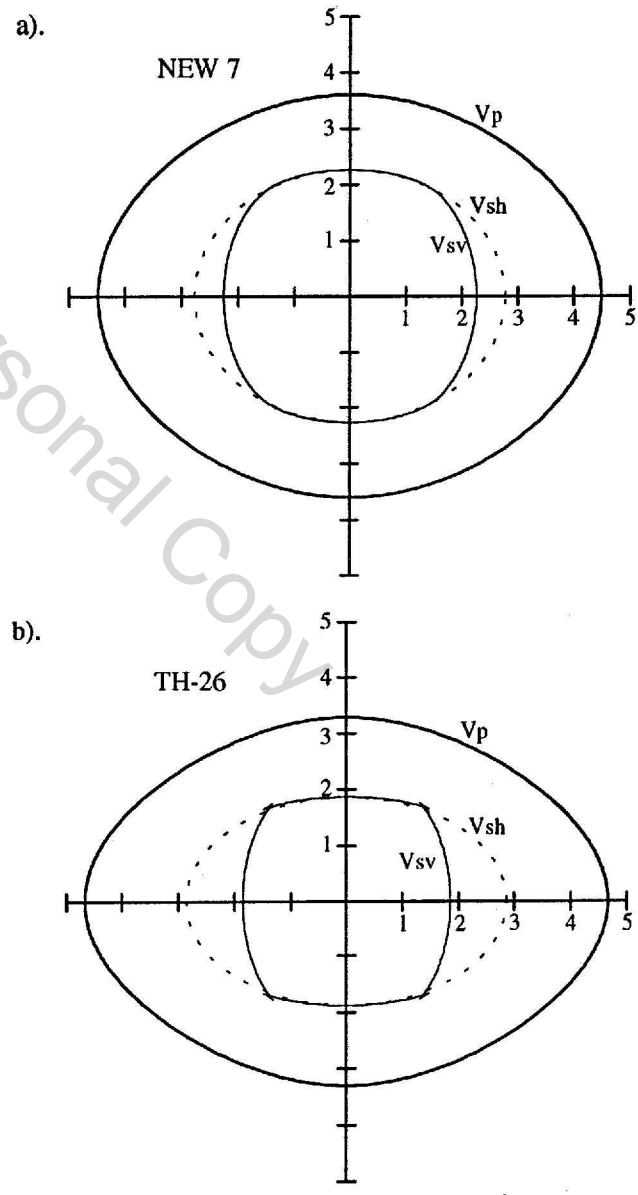

Figure 16. Group velocity surfaces for (a) NEW7 and (b) TH-26. Vertical axes are velocities perpendicular to bedding (in km/s), horizontal axes are velocities parallel to bedding.

locity measurements on multiple cores to ensure that representative elastic constants are obtained. The elastic constants can then be used to calculate velocity surfaces, which when constrained by independent velocity measurements, can provide information concerning wave propagation in highly anisotropic shales important to the interpretation of seismic data. The conclusions of this investigation provide a better understanding of the seismic properties of poorly understood, yet volumetrically and economically significant, sedimentary rocks.

Acknowledgments. Sincere thanks to C. Just of the Lafarge Corp. (Alpena, Michigan) and the Scott County Stone Co. (Scottsburg, Indiana) for permission to collect samples. The assistance of D. Szymanski, N. Levine, G. Schrader, J. Farrell, and J. Bracken in sample collection is appreciated. Many thanks to Roy Wilkens at the Hawaii Institute of Geophysics for obtaining microprobe images of the shales. Thoughtful reviews by F. Paillet and G. Fryer improved the manuscript. This work was supported by the Office of Naval Research contract N00014-89-J-1209 and the National Science Foundation.

References

Auld, B. A., *Acoustic Fields and Waves in Solids*, vol. 1, 435 pp., Robert E. Krieger, Malabar, Florida, 1990.

Banik, N. C., Velocity anisotropy of shales and depth estimation in the North Sea Basin, *Geophysics*, *49*, 1411-1419, 1984.

Boggs, S., Jr., *Petrology of Sedimentary Rocks*, 707 pp., Macmillan, New York, 1992.

Brocher, T. M., and N. I. Christensen, Seismic anisotropy due to preferred mineral orientation observed in shallow crustal rocks in southern Alaska, *Geology*, *18*, 737-740, 1990.

Carlson, R. L., C. H. Schaftenaar, and R. P. Moore, Causes of compressional wave anisotropy in carbonate-bearing deep-sea sediments, *Geophysics*, *49*, 525-532, 1984.

Carrion, P., J. Costa, J. E .F. Pinheiro, and M. Schoenberg, Cross-borehole tomography in anisotropic media, *Geophysics*, *57*, 1194-1198, 1992.

Castagna, J. P., M. L. Batzle, and R. L. Eastwood, Relationships between compressional wave and shear wave velocities in clastic silicate rocks, *Geophysics*, *50*, 571-581, 1985.

Christensen, N. I., Shear wave velocities in metamorphic rocks at pressures to 10 kilobars, *J. Geophys. Res.*, 71, 3549-3556, 1966.

Christensen, N. I., Measurements of dynamic properties of rocks at elevated temperatures and pressures, in *Measurements of Rock Properties at Elevated Pressures*, edited by H.J. Pincus, and E.R. Hoskins, pp. 93-107, American Society for Testing and Materials, Philadelphia, Pa., 1985.

Christensen, N. I., and D. L. Szymanski, Seismic properties and origin of reflectivity from a classic Paleozoic sedimentary sequence, Valley and Ridge province, southern Appalachians, *Geol. Soc. Am. Bull.*, *103*, 277-289, 1991.

Dellinger, J., and L. Vernik, Do traveltimes in pulse transmission experiments yield anisotropic group or phase velocities?, *Geophysics*, *59*, 1774-1779, 1994.

Folk, R. L., Petrography and origin of the Silurian Rochester and McKenzie Shales, Morgan County, West Virginia, *J. Sediment. Petrol.*, *32*, 539-578, 1962.

Freund, D., Ultrasonic compressional and shear velocities in dry clastic rocks as a function of porosity, clay content, and confining pressure, *Geophys. J. Int.*, *108*, 125-135, 1992.

Gipson, M., Jr., Application of the electron microscope to the study of particle orientation and fissility in shale, *J. Sediment. Petrol.*, *35*, 408-414, 1965.

Gipson, M., Jr., A study of the relations of depth, porosity, and clay mineral orientation in Pennsylvanian shales, *J. Sediment. Petrol.*, *36*, 888-903, 1966.

Hasenmueller, N. R., and J. L. Basset, Stratigraphy of the New Albany shale, in *Studies of the New Albany Shale (Devonian and Mississippian) and Equivalent Strata in Indiana*, edited by N. R. Hasenmueller, and G. S. Woodard, pp. 5-32, Indiana Geological Survey, Bloomington, 1981.

Hearmon, R. F. S., *An Introduction to Applied Anisotropic Elasticity*, 136 pp., Oxford University Press, New York, 1961.

Johnston, J. E., and N. I. Christensen, Shear wave reflectivity, anisotropies, Poisson's ratios, and densities of a southern Appalachian Paleozoic sedimentary sequence, *Tectonophysics*, *210*, 1-20, 1992.

Johnston, J. E., and N. I. Christensen, Elastic constants and velocity surfaces of indurated anisotropic shales, *Surv. Geophys.*, *15*, 481-494, 1994.

Jones, L. E. A., and H. F. Wang, Ultrasonic velocities in Cretaceous shales from the Williston basin, *Geophysics*, *46*, 288-297, 1981.

Kaarsberg, E. A., Introductory studies of natural and artificial aggregates by sound propagation and x-ray diffraction methods, *J. Geol.*, *67*, 447-472, 1959.

Levin, F. K., Seismic velocities in transversely isotropic media, *Geophysics*, *44*, 918-936, 1979.

Lineback, J. A., Stratigraphy of the New Albany Shale in Indiana, *Bull. Indiana Geol. Surv.*, *52*, 1291-1303, 1970.

Lo, T., K. B. Coyner, and M. N. Toksoz, Experimental determination of elastic anisotropy of Berea sandstone, Chicopee shale, and Chelmsford granite, *Geophysics*, *51*, 164-171, 1986.

Lynn, H. B., and L. A. Thomsen, Reflection shear wave data collected near the principal axes of azimuthal anisotropy, *Geophysics*, *55*, 147-156, 1990.

Matthews, R. D., Review and revision of Devonian-Mississippian stratigraphy in the Michigan Basin, in Petroleum Geology of the Devonian and Mississippian Black Shale of Eastern North America, edited by J. B. Roen and R. C. Kepferle, pp. D1-D85, *U.S. Geol. Surv. Bull.*, *1909*, 1993.

Meade, R. H., X-ray diffractometer method for measuring preferred orientation in clays, *U.S. Geol. Surv. Prof. Pap. 424B*, 273-276, 1961.

Moore, D. M., and R. C. Reynolds Jr., *X-Ray Diffraction and the Identification and Analysis of Clay Minerals*, 332 pp., Oxford University Press, New York, 1989.

Musgrave, M. J. P., *Crystal Acoustics*, 288 pp., Holden-Day, Oakland, Calif., 1970.

O'Brien, N. R., Origin of Pennsylvanian underclays in the Illinois Basin, *Bull. Geol. Soc. Am.*, *75*, 823-832, 1964.

O'Brien, N. R., The fabric of shale - An electron microscope study, *Sedimentology*, *15*, 229-246, 1970.

O'Brien, N. R., The effects of bioturbation on the fabric of shale, *J. Sediment. Petrol.*, *57*, 449-455, 1986.

Odom, I. E., Clay fabric and its relation to structural properties in mid-continent Pennsylvanian sediments, *J. Sediment. Petrol.*, *37*, 610-623, 1967.

Podio, A. L., A. R. Gregory, and M. E. Gray, Dynamic properties of dry and water saturated Green River Shale under stress, *Soc. Pet. Eng. J.*, *8*, 389-404, 1968.

Postma, G. W., Wave propagation in a stratified medium, *Geophysics*, *20*, 780-806, 1955.

Rai, C. S., and K. E. Hanson, Shear wave velocity anisotropy in sedimentary rocks: A laboratory study, *Geophysics*, *53*, 800-806, 1988.

Sayers, C. M., The elastic anisotropy of shales, *J. Geophys. Res.*, *99*, 767-774, 1994.

Silverman, E. N., and T. F. Bates, X-ray diffraction study of orientation in Chattanooga Shale, *Am. Mineral.*, *45*, 60-68, 1960.

Thomsen, L. A., Weak elastic anisotropy, *Geophysics*, *51*, 1954-1966, 1986.

Vernik, L., and A. Nur, Ultrasonic velocity and anisotropy of hydrocarbon source rocks, *Geophysics*, *57*, 727-735, 1992.

Walker, K. R. (Ed.), The geologic history of the Thorn Hill Paleozoic section (Cambrian-Mississippian) eastern Tennessee, *Stud.*

in Geol., *10*, 128 pp., Dept. of Geol. Sci., Univ. of Tenn., Knoxville, 1985.

White, J. E., L. Martineau-Nicoletis, and C. Monash, Measured anisotropy in Pierre shale, *Geophys. Prospect.*, 31, 709-725, 1983.

White, S. H., H. F. Shaw, and J. M. Hugget, The use of back-scattered electron imaging for the stratigraphic study of sandstones and shales, *J. Sediment. Petrol.*, *54*, 487-494, 1984.

Winterstein, D. F., Anisotropy effects in P-wave and SH-wave stacking velocities contain information on lithology, *Geophysics*, *51*, 661-672, 1986.

Winterstein, D. F., Velocity anisotropy terminology for geophysicists, *Geophysics*, *55*, 1070-1080, 1990.

N. I. Christensen and J. E. Johnston, Department of Earth and Atmospheric Sciences, Purdue University, 1397 Civil Engineering Building, West Lafayette, IN 47907-1397. (fax: (317) 496-1210)

(Received September 12, 1994; revised December 15, 1994; accepted December 29, 1994.)